Single-Atom Catalysis

DOI: 10.1002/ange.201109065

Catalytically Active Single-Atom Sites Fabricated from Silver Particles**

Zhiwei Huang, Xiao Gu, Qingqing Cao, Pingping Hu, Jiming Hao, Junhua Li, and Xingfu Tang**

Supported silver nanoparticles (SNP) have been successfully used as oxidation catalysts in many chemical reactions, such as ethylene epoxidation, partial oxidation of methanol, and complete oxidation of formaldehyde.[1–3] Both experimental and theoretical results show that one of the important steps in these reactions is activation of oxygen especially at the periphery of the SNP in contact with the support.[4,5] Typically, the amount of the interfacial oxygen plays a crucial role in regulating catalytic activity or/and selectivity, which is in essence associated with the size of Ag particles. This means that catalytic reactions occurring on silver-based catalysts exhibit strongly size-dependent activity.[3,4,6] A recent report revealed that the supported subnanometer-sized Ag_3 clusters show much higher catalytic activity than the SNP of about 3.5 nm in propylene epoxidation.[4] Therefore, downsizing SNPs to clusters or even to single atoms is highly desirable for enhancement of catalytic activity.[7] However, a great challenge encountered with the use of single-atom metal on oxide supports is that single atoms are prone to sintering during reactions, leading to a decrease of their catalytic performance.[4,8]

Herein we present the fabrication of the single-atom Ag chains from SNPs supported on Hollandite-type manganese oxide (HMO) nanorods. The Ag atoms of the SNP were initially dispersed and then thermally migrated along the external surfaces to the ends of the HMO nanorods, and were consecutively inserted in the tunnels of the HMO to form single-atom Ag chains, resulting in single Ag atoms anchored at the tunnel openings of the HMO. This single-atom Ag catalyst exhibited excellent activation ability to both lattice oxygen and molecule dioxygen at low temperatures.

[*] Z. Huang,[+] Dr. X. Gu,[+] Q. Cao,[+] P. Hu, Prof. X. Tang
Department of Environmental Science and Engineering
Fudan University, 220 Handan Road, Shanghai, 200433 (China)
E-mail: tangxf@fudan.edu.cn

Q. Cao,[+] Prof. J. Hao, Prof. J. Li
School of Environment
Tsinghua University, Beijing, 100084 (China)
E-mail: lijunhua@tsinghua.edu.cn

[+] These authors contributed equally to this work.

[**] This work was financially supported by the NSFC (20977018 and 21077026). We thank Prof. F. Kapteijn from Delft University of Technology for valuable discussion, and Prof. Y. Huang, Dr. S. Zhang, and Dr. Z. Jiang from SSRF, Chinese Academy of Sciences, and Prof. S. Wei from NSRL, University of Science and Technology of China, for their help in the XAS measurements and data analysis.

Supporting information for this article is available on the WWW under http://dx.doi.org/10.1002/anie.201109065.

The synthesized HMO has a nanorod-shaped morphology, grows along a [001] direction, and exposes the most stable {110} side-facets and the {001} top-facets (Supporting Information, Figure S1). The HMO has one-dimensional $0.47 \times 0.47\ nm^2$ square tunnels, and the basic unit of the tunnel structure is built by eight $(4+4)$ oxygen atoms to form a tetragonal prism.[9] Each of the eight oxygen atoms in the tunnels has four sp^3-hybridized orbitals, three of which bond to three Mn^{4+} cations and another occupied by lone-pair electrons points to the central axis of the tunnel. Theoretically, specially sized linear tunnels and electron-rich tunnel oxygen atoms serving as a natural mold and an electron donor, respectively, favor formation of stable single-atom Ag chains in the tunnels of the HMO.[9,10] In fact, the presence of electron donors such as oxygen or nitrogen atoms have been shown to favor the formation of Ag metallic chains.[11,12]

As a prelude to synthesis of single-atom Ag chains, the SNPs were initially supported on the external surfaces of the HMO to obtain Ag/HMO. As shown in the transmission electron microscopy (TEM) images (Figure 1 a,b), SNPs with an average size of about 3.6 nm (1.6 nm in height and 4.8 nm in diameter) are highly dispersed on the surface of the HMO. When viewed along a $[111]_{Ag}$ direction of the SNP (the subscript represents the Miller index of the SNP), a hexagonal image closed by two $\{100\}_{Ag}$ facets and four $\{111\}_{Ag}$ facets can be observed in the high-resolution TEM (HRTEM) image of Figure 1 c,[13] corroborated by the HRTEM image of the SNP in Figure 1 d. The SNP can therefore be considered as a truncated-octahedral shape. According to the lattice fringe analyses from the HRTEM images in Figure 1 c,d, the crystallographic orientation relationship between the SNP and the HMO shows that the $\{111\}_{Ag}$ facet of the SNP parallels the {110} one of the HMO,[13–16] as shown in the model in Figure 1 e.

The Ag-HMO was obtained by annealing the Ag/HMO, and judging from the smooth surfaces of the TEM images in Figure 1 f,g, the SNPs of Ag/HMO vanish in the Ag-HMO. Noticeably, single-atom linear chains are clearly seen in the HRTEM image (Figure 1 h), which are absent in the HRTEM image of the HMO (Supporting Information, Figure S1d); combined with the elemental analysis data (Supporting Information, Table S1), it is evident that the single-atom linear chains are constructed by the Ag atoms. The positions of the Ag atoms in the chains can be more clearly identified in Figure 1 i, which is obtained from the HRTEM image in Figure 1 h using the auto-correlation function technique.[17] Therefore, the results indicate that the single-atom Ag chains have been successfully synthesized by the simple thermal processing. The HRTEM image matches well with an image

© 2012 Wiley-VCH Verlag GmbH & Co. KGaA, Weinheim

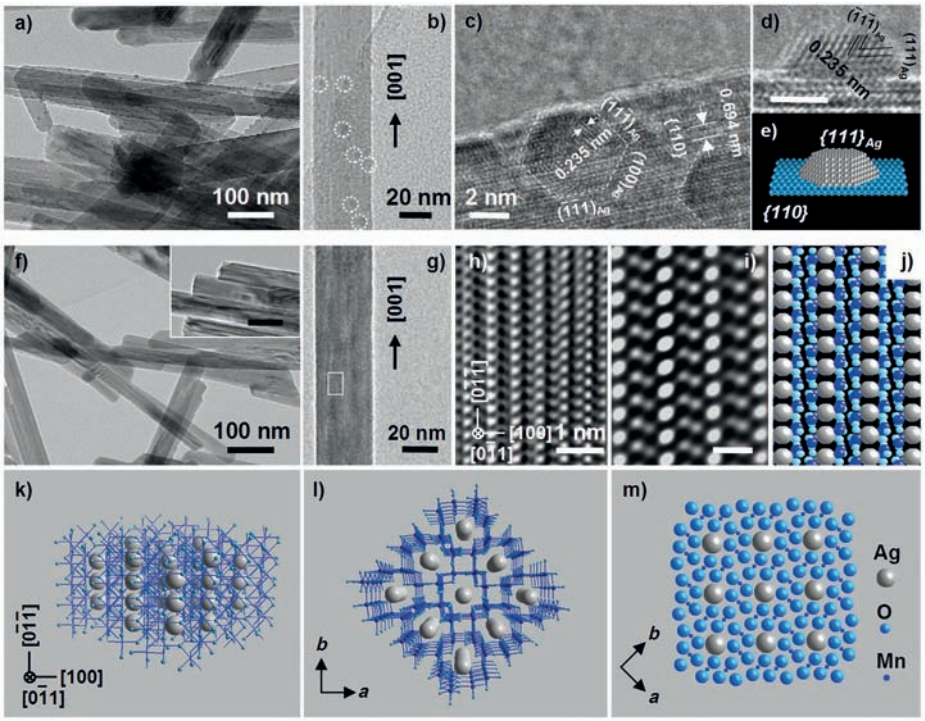

Figure 1. TEM and HRTEM images and the corresponding structural models of Ag/HMO and Ag-HMO. a) TEM image of Ag/HMO. b) TEM image of the SNP (white dotted circles) supported on a typical HMO nanorod with a [001] growth direction. c) HRTEM image of the Ag/HMO showing a hexagonal SNP. d) HRTEM image of the Ag particle of Ag/HMO. e) Structural model of the Ag particle supported on the {110} side-facet of the HMO. f) TEM images of Ag-HMO. Inset: TEM image of Ag-HMO showing flat {001} facets at the ends of Ag-HMO nanorods (scale bar: 50 nm). g) TEM image and h) HRTEM image of a Ag-HMO nanorod with a [001] growth direction, indicating the Ag atom chains. i) Auto-correlation function analysis and j) simulated images of the panel (h) showing Ag single-atom chains. Scale bar: 0.5 nm in the panel (i). k,l) Single-atom Ag chains inside the tunnels of the HMO viewed from the [0$\bar{1}$1] and [001] directions, respectively. m) Atom arrangement on the {001} facet of Ag-HMO.

of the atom arrangement of the {0$\bar{1}$1} plane in the reported silver HMO.[18] It is possible that Ag-HMO has a similar structure, which can be described as several models (Figure 1j–m). However, the position of the single-atom Ag chain is still an issue: in the internal tunnel, or on the external surface, or both.

To shed light on the formation and position of the single-atom Ag chains, temperature-dependent in situ X-ray diffraction (XRD) and room-temperature XRD patterns were obtained. The in situ XRD patterns of Ag/HMO are recorded at 50 °C intervals (Figure 2a; Supporting Information, Figure S2). The diffraction peaks of both the HMO and metal Ag simultaneously appear in the XRD pattern of the Ag/HMO at 80 °C. Upon increasing the temperature up to 230 °C, the diffraction intensity of the (111) plane of the SNP gradually decreases and its location shifts to lower Bragg angles, and with further increasing the temperature the reflection of the metal Ag vanishes. The hollandite crystal structure remains unchanged in the whole process except for slight modifications of the intensity and location of the reflections, and no new reflections arise (Supporting Information, Figure S2). It can be speculated that the Ag atoms have migrated along the surface and are highly dispersed on/in the HMO, which is consistent with the (HR)TEM observations.

The modification of the HMO structure owing to the addition of Ag was monitored in detail by comparing room-temperature XRD patterns of the Ag-HMO with the HMO (Figure 2b; Supporting Information, Figure S3). No reflections owing to Ag species such as metal Ag, Ag_2O and AgO appear in the XRD pattern of the Ag-HMO, which is indicative of highly dispersed Ag species. The diffraction intensity of the HMO is modified by the addition of Ag, and the reflections of the (220), (310), and (420) planes become stronger, while those such as the (211), (301), and (411) planes are weaker. These effects probably originate from influence of the structure factor on diffraction intensity, assuming that the $(0,0,^1/_2)$ sites in the tunnels of the HMO are occupied by Ag atoms.[18,19] The reflections of the (110), (200), and (002) planes are also considerably weakened, which possibly results from restructuring of the atoms in these planes and/or from deviation of the atoms from these planes owing to the addition of Ag. The results are consistent with the fact that the higher the Ag content in the tunnel, the weaker the reflections of these planes for the reported silver HMO.[20]

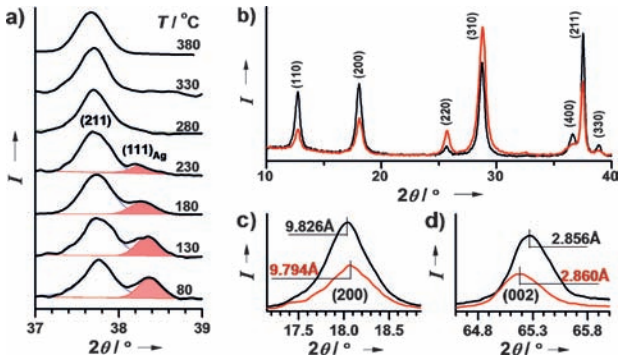

Figure 2. a) In situ XRD patterns of Ag/HMO at different temperatures. The shaded areas represent the (111) reflections of the SNP. b) Room-temperature XRD patterns of HMO (black) and Ag-HMO (red). c,d) Lattice parameters of *a* and *c* calculated from the (200) and (002) diffraction peaks of HMO (black) and Ag-HMO (red), respectively.

© 2012 Wiley-VCH Verlag GmbH & Co. KGaA, Weinheim

The crystal structure of HMO has been thoroughly characterized.[19,21] When the HMO tunnels are occupied by Ag atoms on the consecutive $(0,0,{}^{1}/_{2})$ sites along the *c* axis, the structure of the HMO is slightly modified. Depending on Miller indices of the planes, the reflections of the Ag-HMO deviate from the corresponding reflections of the HMO. Typically, the (200) peak of Ag-HMO shifts to a slightly higher Bragg angle, leading to a smaller *a* lattice parameter (9.794 Å) than that (9.826 Å) of the HMO (Figure 2c). In contrast, the (002) peak of Ag-HMO shifts to a lower Bragg angle (Figure 2d). The *c* lattice parameter (2.860 Å) of Ag-HMO is slightly larger than the value (2.856 Å) of HMO. As a consequence, it is impossible that all of the Ag atoms are only dispersed on the external surfaces of the HMO, and if this is the case, the crystal parameters of the HMO would remain unchanged. Evidently, the single-atom Ag chains of the SNP have been partly or completely inserted into the tunnels of the HMO on the basis of the XRD patterns.

The immediate environments of the Ag atoms were investigated by using the X-ray adsorption spectroscopy (XAS) covering both X-ray absorption near-edge structure (XANES) and extended X-ray absorption fine structure (EXAFS) spectroscopes. Figure 3a shows the Fourier transform (FT) amplitudes of the $\chi(R)$ k^2-weighted EXAFS data at the Ag K-edge of the samples, and the structural parameters were obtained by fitting the spectra with theoretical models and are summarized in Table 1.[18] The *k*-space spectra, curve-fitting of *R*-space, and inverse FT spectra are given in the Supporting Information, Figures S4–S8. The similarity between the FT spectra of the Ag/HMO and the Ag foil elucidates that the local environments of their Ag atoms are similar to each other. The first shell in the FT spectra of the Ag/HMO represents the nearest-neighbor Ag–Ag coordination sphere with an average distance of about 2.87 Å and coordination number of 10, indicating that the metal SNP is present in the Ag/HMO, which is consistent with the XRD patterns and the HRTEM observations. The distinctly different FT spectrum of the Ag-HMO from the spectrum of the Ag/HMO shows a great change of the Ag local geometry. The first shell in the FT spectra of Ag-HMO, with a distance of about 2.33 Å, can be assigned to the Ag–O bonds, which are much longer than the Ag–O bond (2.04 Å) in Ag_2O (Table 1) and shorter than the value (ca. 2.50 Å) of the Ag–O distance in Ag_2SO_4. The Ag–O bond in Ag-HMO is also slightly shorter than the Ag^{+}–O^{2-} distance (2.44 Å) of the reported silver HMO.[18] Judging from the *a* lattice parameter of Ag-HMO, which is slightly larger than the corresponding parameter of silver HMO (9.794 Å vs. 9.726 Å), the Mn–O bond of the Mn-O-Ag bridge in Ag-HMO becomes longer owing to Jahn–Teller distortation of the MnO_6 octahedra.[22] The average Ag–Ag distance (ca. 2.83 Å) of Ag-HMO is 1–2% shorter than that (2.87 Å) for Ag/HMO or 2.89 Å for Ag foil, which is also much shorter than a similar oxygen-supported Ag^{+}–Ag^{+} bond (2.934 Å) owing to strong electrostatic repulsion between Ag^{+} cations.[23]

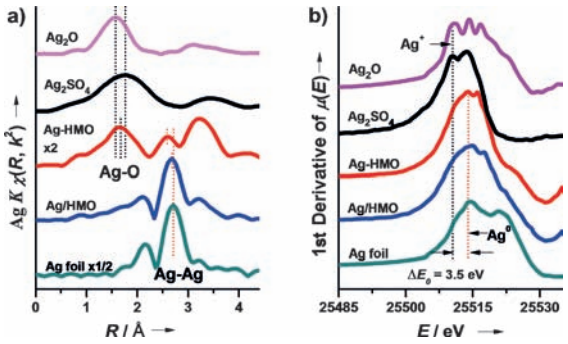

Figure 3. a) $\chi(R)$ k^2-weighted Fourier-transform EXAFS spectra and b) First derivatives of the Ag K-edge XANES spectra of the Ag-HMO, the Ag/HMO, and the Ag foil, Ag_2SO_4, and Ag_2O.

Table 1: Local structure parameters around silver estimated by EXFAS analysis.

Sample	Shell	N[a]	R [Å][b]	σ^2 [Å^2][c]	ΔE_0 [eV][d]
Ag-HMO	Ag-O	4	2.33(1)	0.025(1)	−0.5
	Ag-Ag	2	2.83(1)	0.017(1)	−0.5
Ag/HMO	Ag-Ag	10	2.87(1)	0.014(1)	−0.5
Ag foil	Ag-Ag	12	2.89(1)	0.012(1)	+3.1
Ag_2O	Ag-O	2	2.04(1)	0.005(2)	+3.5
	Ag-Ag	12	3.31(3)	0.012(2)	+3.5

[a] N = coordination number. [b] R = distance between absorber and backscatter atoms. [c] σ^2 = Debye–Waller factor. [d] ΔE_0 = energy shift; *R*-space fit, Δk = 2.4–11.8 Å^{-1}, Δr = 1.2–4.0 Å.

The first shell in the FT spectra of Ag-HMO, with a distance of about 2.33 Å, can be assigned to the Ag–O bonds, which are much longer than the Ag–O bond (2.04 Å) in Ag_2O (Table 1) and shorter than the value (ca. 2.50 Å) of the Ag–O distance in Ag_2SO_4. The Ag–O bond in Ag-HMO is also slightly shorter than the Ag^{+}–O^{2-} distance (2.44 Å) of the reported silver HMO.[18] Judging from the *a* lattice parameter of Ag-HMO, which is slightly larger than the corresponding parameter of silver HMO (9.794 Å vs. 9.726 Å), the Mn–O bond of the Mn-O-Ag bridge in Ag-HMO becomes longer owing to Jahn–Teller distortation of the MnO_6 octahedra.[22] The average Ag–Ag distance (ca. 2.83 Å) of Ag-HMO is 1–2% shorter than that (2.87 Å) for Ag/HMO or 2.89 Å for Ag foil, which is also much shorter than a similar oxygen-supported Ag^{+}–Ag^{+} bond (2.934 Å) owing to strong electrostatic repulsion between Ag^{+} cations.[23]

Taking the coordination number of 2 at the Ag–Ag shell of the Ag-HMO into account (Table 1), there are in principle two possible coordination environments: a single-atom Ag chain and a Ag trimer.

There are still two possible locations for a single-atom Ag chain: the exposed {110} surfaces and the internal tunnels of the HMO. Accordingly, we have calculated adsorption energy for the Ag atom for both cases (Supporting Information, Figure S9). Two kinds of surfaces are concerned: one is oxygen-lean and the other is oxygen-rich. The adsorption energy for the Ag atoms on the oxygen-lean (110) surface is about 1.0 eV higher than the internal case. For the oxygen-rich surface where all the manganese atoms on the (110) surface are supposed to be saturated by oxygen ions, the adsorption energy for the Ag atom is still higher than that inside the tunnels. The results indicate that the single Ag atoms in the tunnel sites are energetically more favorable than ones on the external {110} surface of the HMO owing to a strong interaction between Ag atoms and tunneled oxygen.[22]

Although a Ag trimer is not observed in the HRTEM image, we have carried out calculations to investigate the possibility of Ag trimer deposited on the {001} top facets (the open terminals of the tunnels) of the HMO owing to the surface energy of the {001} top facets being higher than the {110} side facts. The results with relaxation show that it is not energetically favorable, and the total energy is about 1.2 eV higher than the corresponding value of a single-atom Ag–Ag–Ag chain inside the tunnel. The results suggest that the possible Ag trimers are not preferred on the {001} top facets when the tunnels are still unoccupied. Furthermore, accord-

© 2012 Wiley-VCH Verlag GmbH & Co. KGaA, Weinheim

ing to detailed calculations (Supporting Information, Section 1.1), the HMO can provide the tunnel sites enough to accommodate all of the Ag atoms of the Ag/HMO. Therefore, it is reasonable to deduce that SNPs in Ag/HMO have been transformed into single-atom Ag chains by annealing, which are completely inserted in the internal tunnels of Ag-HMO (shown as models in Figure 1k,l).

According to the EXAFS results, Ag-HMO has much longer Ag–O and much shorter Ag–Ag distances than the corresponding distances of Ag_2O, indicating that the SNP of Ag/HMO did not transform into Ag_2O in the preparation of Ag-HMO, but the oxidation state of Ag in Ag-HMO is under debate. Ag K-edge XANES spectroscopy and X-ray photoelectron spectroscopy (XPS) have been exploited to determine the oxidation state of Ag. Figure 3b shows the first derivatives of the Ag K-edge XANES spectra for the Ag-HMO and Ag/HMO together with three references, and the corresponding XANES spectra are given in the Supporting Information, Figure S10. The first maximum value in the first derivative spectra ascribed to absorption threshold energy (E_0) is located at about 25514.3 eV for both Ag-HMO and Ag/HMO, which is close to the E_0 value of Ag foil (Ag^0), and 3.5 eV higher than the E_0 value of Ag_2O or Ag_2SO_4. The negative shifts of absorption energy with increasing oxidation state of Ag have been substantiated in Ag L-edge XANES spectra.[24,25] The results suggest that the Ag species of Ag-HMO is probably a metallic state ($Ag^{\delta+}$, $0<\delta<1$), which is consistent with the XPS results (Supporting Information, Figures S11,12, Table S2, and the related discussion in Section 1.6). Similarly, the Ag species in the reported Ag_2MnO_2 crystalline sample retained partly metallic state ($Ag^{\delta+}$, $\delta = {}^1/_2$), which was prepared using a solid-state reaction technique with a stoichiometric mixture of Ag metal and MnO_2 powder and sequentially subjected to calcine at 650 °C in an oxygen flow for 24 h.[26] Combining all of the above results with the related discussion, the evidence supports the formation of single-atom $Ag^{\delta+}$ linear chains in the tunnels of the HMO. According to the appropriate amount of Ag (Supporting Information, Section 1.1) and the forthcoming HCHO oxidations, the single-atom chains probably expose single Ag atoms on the tunnel openings of HMO, as shown in Figure 1m. Thus, Ag-HMO with exposed single $Ag^{\delta+}$ atoms as a model catalyst should readily activate oxygen species at low temperatures.[4,7]

The activation of oxygen over Ag, including both lattice oxygen and molecule oxygen, has been proven crucial for many oxidation reactions at low temperatures.[5,27] Xia et al.[27] reported that the addition of Ag could activate lattice oxygen of the HMO owing to electron transfer from Mn^{3+} to Ag^+ through the Zener exchange by the Ag–O–Mn-bridged oxygen atom, which enhanced the catalytic activity towards CO oxidation at $T \le 100$ °C. The results demonstrated that the activated ability of the catalytically active sites towards oxygen is intimately associated with the catalytic performance. The Ag clusters are considerably facile for molecule O_2 dissociation, which is often the rate-determining step in oxidation reactions.[5,28,29] Essentially, a linear Brønsted–Evans–Polanyi relation between activation energy of O_2 dissociation and reaction energy has been established for many oxidation reactions occurring on metal surfaces.[29,30]

The activation ability of the Ag-HMO towards oxygen is evaluated by complete oxidation of HCHO owing to the instinct activity of silver towards the HCHO oxidation at low temperatures[3,31] (Supporting Information, Figure S13). Ag-HMO has considerable catalytic activity for complete oxidation of HCHO at $T \le 80$ °C, reflecting that Ag-HMO exhibits excellent activation ability of oxygen, whereas under the same reaction conditions the HMO is not active, which is indicative of HCHO reactions merely occurring on the Ag sites of Ag-HMO at $T \le 80$ °C. Owing to the diameter of O_2 (3.46 Å) being much larger than the effective pore openings (ca. 2.65 Å) of the Ag-HMO,[32] O_2 cannot be inserted in the internal tunnels to complete the HCHO oxidation cycles, that is, HCHO oxidation only occurs on the external surfaces of Ag-HMO. These results strongly suggest that single-atom Ag chains exposing single Ag atoms on the {001} top-facets of Ag-HMO nanorods are the catalytically active sites for HCHO oxidation.

A reaction rate in terms of a turnover frequency (TOF, number of converted HCHO molecules per surface Ag active site per second) is shown in Figure 4a. The surface active sites

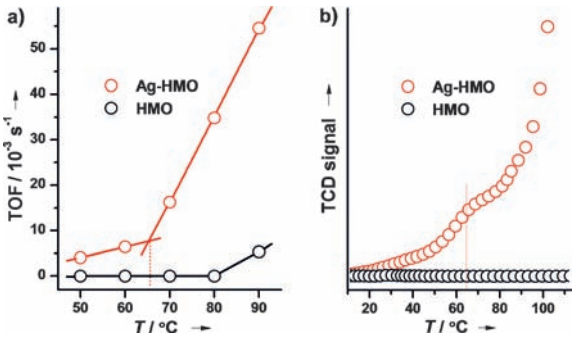

Figure 4. a) TOF in the HCHO oxidation and b) H_2-TPO profiles of Ag-HMO and HMO.

of Ag-HMO are defined to be the single Ag atoms anchored at the openings of the tunnels of the Ag-HMO nanorods. On the basis of the above discussion and the amount of Ag, it is reasonable to assume that the opening sites of the tunnels on the {001} top facets of the Ag-HMO nanorods are completely occupied by the Ag atoms, as in the model in Figure 1m. The definitions and detail calculations about the catalytically active sites of the Ag-HMO, Ag/HMO and HMO are given in the Supporting Information, Section 1.8. HCHO oxidation evidently shows a temperature dependency. The TOF of Ag-HMO is 0.004 s^{-1} at 50 °C, which gradually increases to 0.006 s^{-1} at 60 °C. Upon increasing temperatures beyond 60 °C, the TOF of Ag-HMO rapidly increases up to about 0.054 s^{-1} at 90 °C, which is 9 times more than the TOF at 60 °C and 11 times more than the HMO at 90 °C. At $T = 80$ °C, the TOF (ca. 0.035 s^{-1}) of Ag-HMO is approximately 7 times more than the corresponding Ag/HMO (ca. 0.005 s^{-1}) by assuming that the Ag atoms at the perimeter of the SNP that are in contact with the HMO are the catalytically active sites (Supporting Information, Sections 1.8.1 and 1.8.2). In comparison, the previously reported Ag catalyst for HCHO

 © 2012 Wiley-VCH Verlag GmbH & Co. KGaA, Weinheim

oxidation at 220 °C has a TOF of 0.004 s^{-1},[3] which is much lower than the Ag-HMO catalyst at low temperatures. Thus, the catalytic activity of Ag-HMO for HCHO oxidation indicates that it has excellent activation ability of both lattice oxygen and molecule oxygen.

There are possibly different mechanisms of oxygen activation at different reaction temperatures for the above reactions. Behm et al.[33] intensively studied the nature of the catalytically active oxygen species in the oxidation of CO over a Au/TiO_2 catalyst and proposed a metal-assisted Mars–van Krevelen mechanism: at $T \leq 80$ °C, only the activated surface lattice oxygen species present at the perimeter of the $Au\text{-}TiO_2$ interface were responsible for the CO oxidation, which could be replenished by dissociative adsorption of O_2 at the perimeter sites; at $T > 80$ °C, migration of surface lattice oxygen and surface oxygen vacancies also gave assess to neighboring surface lattice oxygen. The mechanism can be possibly applied to the Ag-HMO described herein. Consequently, two straight lines that can be drawn to represent the catalytic activity as a function of temperature meet at about 65 °C (Figure 4a). Presumably, at $T \leq 65$ °C, the HCHO oxidation on the Ag-HMO also follows a similar silver-assisted Mars–van Krevelen mechanism, where the only oxygen at the perimeter sites of the single Ag atom can be activated to react with HCHO; at $T > 65$ °C, the mechanism of oxygen activation is possibly same as the Au/TiO_2 at $T >$ 80 °C.

To substantiate the above mechanism of the oxygen activation on the Ag-HMO, we focus on activation of the lattice oxygen using H_2 as a probe molecule by temperature-programmed oxidation of H_2 (H_2-TPO, Figure 4b; Supporting Information, Figure S14). The lattice oxygen of HMO is not active in the H_2 atmosphere at $T \leq 180$ °C, whereas Ag-HMO is active for H_2 oxidation at temperatures more than 20 °C, and incidentally at about 65 °C, the first peak in the H_2-TPO profile is discernible, which is possibly due to the H_2 consumption by lattice oxygen at the perimeters of the exposed single-atom Ag active sites. At $T > 90$ °C, the rate of the H_2 oxidation by the lattice oxygen is rapidly increased to reach a maximum at about 120 °C. It appears to be true that the H_2 consumption originates from its reaction with the lattice oxygen directly adjacent to the single-atom Ag chains in the Ag-HMO tunnels. The phenomenon can be attributed to H_2 dissociation on the exposed single-atom Ag and spillover of H atoms along the single-atom Ag chains,[34] which is not observed at this temperature region in the H_2-TPO profile of the Ag/HMO under the same conditions (Supporting Information, Figure S14). The high rate of the H_2 oxidation is closely associated with the high coordination number of the Ag to lattice oxygen and the structure feature of the single-atom Ag chains. Therefore, the single-atom Ag (chain) has excellent activation ability towards oxygen at low temperatures, which possibly results from a strong metal–support interaction between single-atom Ag and the lattice oxygen through hybridization of O 2p levels with Ag 4d and Ag 5sp orbitals.[10]

In summary, single-atom Ag chains were successfully synthesized by simple thermal processing of Ag particles and were substantiated by various characterization techniques, such as HRTEM, XRD, and XAS. The amount of Ag was elaborately designed to allow single-atom Ag chains to expose the terminal Ag atoms on the openings of the Ag-HMO tunnels to form single-atom catalytically active sites. This single-atom Ag catalyst showed high activation ability to both lattice oxygen and molecule oxygen, which resulted in excellent activity in the HCHO oxidation at low temperatures. Further studies are underway to find out the mechanism of single-atom Ag chain formation.

Received: December 22, 2011
Published online: March 14, 2012

Keywords: formaldehyde · heterogeneous catalysis · manganese oxide · oxidation · silver

[1] M. A. Barteau, R. J. Madix, *J. Am. Chem. Soc.* **1983**, *105*, 344.
[2] T. Mallat, A. Baiker, *Chem. Rev.* **2004**, *104*, 3037.
[3] C. F. Mao, M. A. Vannice, *J. Catal.* **1995**, *154*, 230.
[4] Y. Lei, F. Mehmood, S. Lee, J. Greeley, B. Lee, S. Seifert, R. E. Winans, J. W. Elam, R. J. Meyer, P. C. Redfern, D. Teschner, R. Schlogl, M. J. Pellin, L. A. Curtiss, S. Vajda, *Science* **2010**, *328*, 224.
[5] A. Wittstock, V. Zielasek, J. Biener, C. M. Friend, M. Baumer, *Science* **2010**, *327*, 319.
[6] S. V. Tsybulya, G. N. Kryukova, S. N. Goncharova, A. N. Shmakov, B. S. Balzhinimaev, *J. Catal.* **1995**, *154*, 194.
[7] B. T. Qiao, A. Q. Wang, X. F. Yang, L. F. Allard, Z. Jiang, Y. T. Cui, J. Y. Liu, J. Li, T. Zhang, *Nat. Chem.* **2011**, *3*, 634.
[8] A. Uzun, V. Ortalan, N. D. Browning, B. C. Gates, *J. Catal.* **2010**, *269*, 318.
[9] M. M. Thackeray, *Prog. Solid State Chem.* **1997**, *25*, 1.
[10] W. H. A. Thijssen, D. Marjenburgh, R. H. Bremmer, J. M. van Ruitenbeek, *Phys. Rev. Lett.* **2006**, *96*, 026806.
[11] B. H. Hong, S. C. Bae, C. W. Lee, S. Jeong, K. S. Kim, *Science* **2001**, *294*, 348.
[12] H. R. Moon, C. H. Choi, M. P. Suh, *Angew. Chem.* **2008**, *120*, 8518; *Angew. Chem. Int. Ed.* **2008**, *47*, 8390.
[13] Z. L. Wang, *Adv. Mater.* **1998**, *10*, 13.
[14] C. H. Chen, L. Jin, A. E. Espinal, B. T. Firliet, L. P. Xu, M. Aindow, R. Joesten, S. L. Suib, *Small* **2010**, *6*, 988.
[15] A. E. Espinal, L. C. Zhang, C. H. Chen, A. Morey, Y. F. Nie, L. Espinal, B. O. Wells, R. Joesten, M. Aindow, S. L. Suib, *Nat. Mater.* **2010**, *9*, 54.
[16] C. Wang, L. Sun, Q. Q. Cao, B. Q. Hu, Z. W. Huang, X. F. Tang, *Appl. Catal. B* **2011**, *101*, 598.
[17] M. Pan, *Micron* **1996**, *27*, 219.
[18] F. M. Chang, M. Jansen, *Angew. Chem.* **1984**, *96*, 902; *Angew. Chem. Int. Ed. Engl.* **1984**, *23*, 906.
[19] B. Dawson, *Proc. R. Soc. London Ser. A* **1967**, *298*, 255.
[20] L. Y. Li, D. L. King, *Chem. Mater.* **2005**, *17*, 4335.
[21] J. Vicat, E. Fanchon, P. Strobel, D. T. Qui, *Acta Crystallogr. Sect. B* **1986**, *42*, 162.
[22] S. Ji, E. J. Kan, M. H. Whangbo, J. H. Kim, Y. Qiu, M. Matsuda, H. Yoshida, Z. Hiroi, M. A. Green, T. Ziman, S. H. Lee, *Phys. Rev. B* **2010**, *81*, 094421.
[23] M. L. Tong, X. M. Chen, B. H. Ye, L. N. Ji, *Angew. Chem.* **1999**, *111*, 2376; *Angew. Chem. Int. Ed.* **1999**, *38*, 2237.
[24] A. V. Kolobov, A. Rogalev, F. Wilhelm, N. Jaouen, T. Shima, J. Tominaga, *Appl. Phys. Lett.* **2004**, *84*, 1641.
[25] S. H. Liu, H. M. Tsai, C. W. Pao, J. W. Chiou, D. C. Ling, W. F. Pong, M. H. Tsai, H. J. Lin, L. Y. Jang, J. F. Lee, J. H. Hsu, W. J. Wang, C. J. Hsu, *Appl. Phys. Lett.* **2006**, *89*, 092112.

 © 2012 Wiley-VCH Verlag GmbH & Co. KGaA, Weinheim

[26] H. Yoshida, S. Ahlert, M. Jansen, Y. Okamoto, J. Yamaura, Z. Hiroi, *J. Phys. Soc. Jpn.* **2008**, *77*, 074719.
[27] G. G. Xia, Y. G. Yin, W. S. Willis, J. Y. Wang, S. L. Suib, *J. Catal.* **1999**, *185*, 91.
[28] J. Hagen, L. D. Socaciu, J. Le Roux, D. Popolan, T. M. Bernhardt, L. Woste, R. Mitric, H. Noack, V. Bonacic-Koutecky, *J. Am. Chem. Soc.* **2004**, *126*, 3442.
[29] H. Falsig, B. Hvolbaek, I. S. Kristensen, T. Jiang, T. Bligaard, C. H. Christensen, J. K. Norskov, *Angew. Chem.* **2008**, *120*, 4913; *Angew. Chem. Int. Ed.* **2008**, *47*, 4835.
[30] T. Bligaard, J. K. Norskov, S. Dahl, J. Matthiesen, C. H. Christensen, J. Sehested, *J. Catal.* **2004**, *224*, 206.
[31] E. M. Stuve, R. J. Madix, B. A. Sexton, *Surf. Sci.* **1982**, *119*, 279.
[32] Z. M. Wang, S. Tezka, H. Kanoh, *Chem. Mater.* **2001**, *13*, 530.
[33] D. Widmann, R. J. Behm, *Angew. Chem. Int. Ed.* **2011**, *50*, 10241.
[34] W. C. Conner, J. L. Falconer, *Chem. Rev.* **1995**, *95*, 759.

 © 2012 Wiley-VCH Verlag GmbH & Co. KGaA, Weinheim